4.5.2.2 Random Turbulence-Induced Vibration

The turbulence-induced vibration analysis is based on Powell's joint acceptance technique (Reference 8), which computes only the RMS vibration amplitude and stresses. The displacements are computed in units of (inch, rms), the moments in units of (in-lbs, rms) and reaction loads at support locations in units of (lbs, rms).

Acceptance Criteria for Displacements

Because the computed displacement response to turbulence is based on a probability of excursions, the displacements (determined in units of inch, rms) are multiplied by a factor of five or five sigma, which represents an approximately 100 percent probability that the computed displacement is not exceeded. The gap clearance between the adjacent CRGA locations is [ ] One-half of this value, [ ] inches, is used as the acceptance criteria to prevent impacts between adjacent CRGAs. Therefore, the allowable displacement in units of inch, rms is [ ] inch/5sigma or [ ] inch, rms for turbulence-induced vibration. Because the transverse displacement of the CRGA column supports exceeds the gap clearance between its ID and the CRGAs, experimental fatigue characterization tests of the CRGAs is performed. The results of the test are reported in Section 4.6.2.

The allowable displacement limit of [ ] inch, rms is conservatively applied to the other column supports (normal and LMP) because the clearance between these components and the CRGA column supports is greater, which is conservative.

Acceptance Criteria for High Cycle Fatigue

The criterion established in Section 4.2.6.2 using fatigue curve “C” is applied to the columns of the upper internals. The allowable stress for fatigue curve “C” at 10^{13} cycles is [ ] psi, rms.

4.5.2.3 Vortex-Shedding Induced Vibrations and RCP Acoustic Pressure Fluctuations

Acceptance Criteria for Displacements

The acceptance criterion for the off resonant response of the column supports assures that the mid-span displacements of the column supports are small enough to avoid impact with adjacent column supports. Because the response to vortex-shedding and the RCP acoustic pressure fluctuations is harmonic, the allowable displacement and the allowable stress are in units of psi (0-peak). As computed for turbulence, the allowable displacement limit for all CRGA column supports is [ ] inch (0-peak).

Acceptance Criteria for High Cycle Fatigue

The ASME fatigue curve "C" shown in Figure 4-21 is applied to the response of the structure. The allowable high cycle fatigue stress of [ ] (0-peak) at 10^{11} cycles for fatigue curve "C."

4.5.3 Response of the Column Supports

The FIV analysis of the column supports and the instrumentation guide tube for the limiting RCP transient condition is performed for fluid-elastic instability. The method by which the full power normal operating conditions are evaluated, considering the 10% RCP transient and a capacity factor of 100% for 60 EFPY, provides a conservative estimate of the total fatigue usage for the high cycle effect created by random turbulence and vortex-shedding such that detailed analysis of this short transient conditions is not necessary.

The full scale theoretical results, considering the sources of excitation identified in Section 4.5.1, are summarized in Table 4-18 through Table 4-20. Figure 4-51 through Figure 4-54 provide the frequency and mode shape plots for the column supports and the instrumentation guide tube. Figure 4-55 through Figure 4-58 provide the displacement response PSD for the same components.

Table 4-18—In-Water Theoretical Natural Frequencies of the Column Supports

[ ]

Table 4-19—Evaluation for Vortex-Shedding Lock-in for the Column Supports

[ ]

Note(s) for Table 4-19:

1. The vortex-shedding frequencies of the column support during the limiting RCP transient with three RCPs operating at cold shutdown conditions are bounded by the vortex-shedding frequencies for the 100 percent power normal operating conditions.
2. See Section 4.5.1.1.2 for details regarding the acceptance criteria for the lock-in condition as provided by the ASME Section III, Appendix N, Paragraph N-1324.1.
3. The FIV results reported in this table are representative of the 10% RCP overspeed transient condition and are a conservative prediction for the 100% full power, steady state, normal operating condition. The exception to this is the FSM results that are reported for the RCP transient condition which is representative of three RCP operation where the flow is reversed through one of the hot leg nozzles. See Section 4.5.1 and Section 4.5.4 for additional details regarding these results.

Table 4-20—Summary of FIV Results for the RV Upper Internal Column Supports

[ ]

Notes for Table 4-20:

1. The stresses reported in this table are based on a conservative FSRF of 3.0 which bounds the computed values for the structural discontinuities of the lower and upper flanges. The full penetration welds used to join the column support parts do not require an FSRF per the ASME Section III requirements; however, a FSRF was conservatively applied.

2. The FIV results reported in this table are representative of the 10% RCP overspeed transient condition and are a conservative prediction for the 100% full power, steady state, normal operating condition. The exception to this is the FSM results that are reported for the RCP transient condition which is representative of three RCP operation where the flow is reversed through one of the hot leg nozzles. See Section 4.5.1 and Section 4.5.4 for additional details regarding these results.

4.5.4 Conclusions

The FIV results reported for the column supports are representative of a 10 percent increase (relative to full power normal operating condition) in the primary flow rate through RV internals or a 10 percent increase in the cross flow velocity profile for the column supports in order to represent the RCP over-speed transient conditions, resulting in a bounding evaluation for the upper internals. These FIV results are evaluated for high cycle fatigue failure considering 60 EFPY with a 100 percent capacity factor. These results meet the FIV acceptance criteria established in Section 4.5.2 for the column supports and bound the HFT (Test #17, See Table 5-4) and the full power, steady state normal operating conditions.

The response of the column supports for the latter two operating conditions can be calculated based upon the ratio of the dynamic pressure term. A scaling factor of [ ] or ([ ]) applied to the results for the 10 percent RCP over-speed transient provides the results consistent with full power, steady state normal operating conditions. A scaling factor of [ ] or [ ] applied to results for the 10 percent RCP over-speed transients provides the results consistent with HFT (Test #17).

The scope of the hot functional testing is defined in Table 5-4 and includes a variety of RCP transients which are performed at different operating temperatures. The RCP transients are normally experienced during plant heatup and have a short duration and the high cycle fatigue resulting from the turbulence is negligible.

The response of the column supports to these RCP transients are measured during HFT to confirm acceptable vibratory behavior based on the acceptance criteria established in Section 4.5.2 to verify that these components do not experience significant amplitudes of vibration and stress. which confirms that the high cycle fatigue resulting from these transients is insignificant. Further, the column supports are observed for the existence of structural damage or abnormal vibrations during these RCP transients while adhering to the acceptance criteria established in Section 5.5 and Section 6.1 of this report.

The development of an analytical response of the column supports to the flow excitations resulting from each of these RCP transient conditions is not required to demonstrate the integrity of these components to the high cycle fatigue concerns associated with these transients.

4.6 CRGAs and RCCAs

The assessment for the vibratory behavior of the CRGAs and the RCCAs is based on full scale flow testing and theoretical analysis. The following test programs are undertaken:

- MAGALY test.
- CRGA modal characterization.
- CRGA fatigue tests.

4.6.1 MAGALY Tests

4.6.1.1 Tests Objectives

A review of the historical operating experiences of previous CRGAs and RCCAs designs show that the in-service operational issues include:

- Wear due to RCCA rod vibrations, which led to loss of rod water tightness, and in the worst cases, to rod breaks.
- Wear induced by vertical step by step motions which could lead to surface adaptations in the CRGA continuous guidance and then to a harmful increase of friction.

The first design issue is resolved by the use of ion nitrited rods. The second design issue is addressed by an improvement of the hydraulic conditions inside the CRGA.

With previous continuous guidance designs, the flows in the CRGA induced pressure differences between the inside and the outside of the continuous guidance channels. These pressure differences would push the RCCA rods along into the slots of the continuous guidance and then induce friction that in some cases increased after surface adaptation.

These two pressure differences are interrelated by the following hydraulic phenomena:

- Low pressure differences in the continuous guidance reduce the friction, but contribute to an increase in the rod vibrations.
- High pressure differences in the continuous guidance limit the rod vibrations, but increase the friction.

Considering these historical issues, the main objective of the MAGALY tests is to find an acceptable compromise between these two phenomena and then validate the redesign.

In the first phase, tests are performed with an adjustable CRGA in order to improve the hydraulic condition within the bottom region of the CRGA. In the second phase, tests are rerun with an actual CRGA design. Therefore, the primary objective of the MAGALY tests is not in the scope of the vibration assessment program of the CRGAs. However, the MAGALY tests are used to assess the flow vibrations of the CRGA in the third phase of the test program.

4.6.1.2 Tests Set-up

The test cell is comprised of hydraulic equipment operating in water at a temperature between 20°C and 40°C (68°F and 104°F) and the full scale length of the reactor control rod drive line (See Figure 4-35 and Figure 4-36). The test loop allows representation of various flow rate conditions:

- Q1 simulates the main axial flow rate in the FA.
- Q2 is the axial flow rate in the fuel guide tubes.
- Q3 simulates the cross flow below the UCP that can exist between neighboring FAs.

- Q4 represents the flow rate exchange between the CRGA and the upper dome.
- Q5 simulates the cross flow that can exist above the UCP and that could influence the flow exit at the CRGA bottom.
- QS1, QS2, QS3, and QS5 are the outflows.

A system of deflectors fixed on the UCP allows the simulation of the various flow conditions outside the CRGA column support resulting from the influence of the neighbouring CRGAs and UCP flow holes that exist at the bottom of the CRGA.

4.6.1.3 Instrumentation

The test loop is instrumented to regulate the following test conditions:

- Inlet and outlet temperature measurements (test temperature 40°C).
- Intake and discharge pressure measurements.
- Measurement of inflows (Q1, Q2, Q3, Q4, and Q5) and outflows (QS1, QS2, QS3, and QS5).

Figure 4-37 presents the instrumentation for the third phase of the MAGALY tests. Several accelerometers and eddy current sensors (displacement measurements) are fixed at the CRGA guide plates to assess the vibration amplitudes.

4.6.1.4 Conclusions

The CRGA responds primarily to its first natural frequency (about [ ] Hz) with an amplitude of [ ] inch, rms for the worst flow condition of the tests, which are performed at [ ] of the nominal flow rate.

Figure 4-35—MAGALY Mock-up

Figure 4-36—MAGALY - Simulated Flow Rates

Figure 4-37—Instrumentation for the Third Phase of MAGALY Tests

4.6.2 CRGA Modal Characterization and Fatigue Tests

4.6.2.1 Test Description

Modal characterization and fatigue tests for the full scale CRGA are performed on a very rigid "CALVA bench" (See Figure 4-38). Modal characterization is performed in air and in still water for the following assembly configurations to assess the influence of the boundary conditions, the hydrodynamic added masses, and the coupling between the upper and lower housings of the CRGA:

- With and without CRGA column.
- With and without upper housing.

The CRGA is equipped with accelerometers at different levels to determine the frequencies and mode shapes. The vibratory fatigue tests are performed in air. The accelerated fatigue tests are carried out according to the rules of experimental stress analysis per RCC-M appendix ZII (French equivalent to ASME Section III, Appendix II rules), considering the vibratory amplitude "A" measured during the MAGALY phase three tests.

During the fatigue tests, the first natural frequency of the CRGA is excited so that the vibratory amplitude "n*A" is obtained, with "n" being the amplification factor determined in accordance to the rules of RCC-M, for the total number of cycles performed during the tests, which is representative of 60 EFPY and a capacity factor of 100 percent.

The CRGA is equipped with accelerometers and strain gauges to detect any drift in its vibratory behavior. At the conclusion of the tests, visual examination and dye penetrant tests are performed to inspect for fatigue damage.

4.6.2.2 Conclusions

No structural damage of the CRGA is detected by visual examination or dye pentrant tests, which followed the fatigue test.

Figure 4-38—CALVA Bench

[ ]

4.6.3 Theoretical Evaluation for the CRGA

A full scale theoretical analysis of the CRGAs is performed for the following components:

- CRGA tie rods.
- CRGA c-tubes (continuous guidance tubes).
- RCCA (when withdrawn into the CRGA).

These analytical evaluations are directed at determining the FIV response of these individual CRGA components, as opposed to tests which evaluate the global response of the CRGA as described in Section 4.6.1 and Section 4.6.2. Based upon the design, arrangement, and flow conditions, the other components of the CRGA, including the guide plates, the main flange, and the RCCA spider are not susceptible to significant flow excitation, Explicit evaluations of these other components are not performed.

The internal components of the CRGA are protected from the extreme cross flow conditions in the upper plenum and the dome by the CRGA column supports. However, the flow through the CRGA column supports between the RV dome and the UCP and vice versa can induce flow excitations of these structures. The flow velocities in the CRGA column supports are minimal above the c-tubes. The entire continuous guidance region in the lower portion of the CRGA (just above the UCP) is hydraulically open and is subjected to the cross flow conditions of the upper plenum.

The flow induced vibration phenomena of concern for these cylindrical shaped structures include:

- Vortex-shedding induced vibration.
- Random turbulence induced vibration due to cross flow.
- Random turbulence induced vibration due to axial flow.

The axial flow through the inside of the CRGA column support is less than [ ] /sec, which is negligible. Due the relatively short spans and the high natural frequencies of the CRGA internal components and the magnitude of axial flow, it is not possible for the turbulent forcing function to become coincident in its phase relationship with the modal frequencies of the CRGA internals to create a significant degree of coherence with the forcing function. Axial flow turbulence-induced vibration is negligible compared with that caused by cross-flow and is not explicitly evaluated for the CRGA internals.

The narrow band acoustic pressure fluctuations associated with the RCP rotational speed ([ ] Hz) and the pump blade passing frequency ([ ] Hz), as well as the other potential sources of acoustic pressure fluctuations (e.g., acoustic resonance and loop acoustics), are not capable of exciting the modal frequencies of the CRGA and the RCCA. This is primarily due to the inability of the long wave length associated with these acoustic pressure fluctuations to impart significant loading on these slender structures, as described in Section 4.5.1.1.5. The measures identified in Section 4.2.5.2.2 for the lower internals verify that sources of acoustic resonance in the RCS piping do not exist.

4.6.3.1 Analysis Methodology and FIV Design Inputs

The analytical methodology implemented for the full scale FIV evaluation of the CRGA internal components is identical to that described for the CRGA column supports in Section 4.5.1.1. There are unique differences in the design inputs for the CRGA internal components, which are defined in this section.

<u>Thermal Hydraulic Inputs</u>

The thermal-hydraulic inputs that are used in the full scale evaluation of the CRGA internals are tabulated in Table 4-21 and are representative of full power normal operating conditions. The thermal-hydraulic inputs are developed from a one dimensional thermal hydraulic model, and the magnitudes are considered nominal. The maximum axial flow velocity through the CRGA column support (**[ ]** ft/sec) is conservatively applied as the cross flow in the CRGA regions above the c-tubes.

<u>Damping for Random Turbulence Vibrations</u>

A viscous damping coefficient of **[ ]** is applied to the CRGA internal components, which is representative of the damping inherent to the material or the hysteresis damping. The structural damping coefficient is set to two times the viscous damping coefficient to achieve the equivalent structural damping at resonance.

<u>Damping for Vortex-Shedding Vibrations (including lock-in conditions)</u>

A total viscous damping value of 0.5% is applied to the tie rods and c-tubes. For the CRGA control rod clusters assemblies, the total viscous damping created by the fluid, hysteresis, and the non-linear interaction of the control rod absorber and the guide plates is itemized in Table 4-34 for the first five modal frequencies. These sources of damping are used to determine the reduced damping value (C_n), which is compared in ASME Code Section III, Appendix N-1324.1, Criteria (c).

<u>Design Inputs for Turbulent Forcing Function</u>

The single phase PSD function, as proposed by Pettigrew and Gorman and also recommended by Reference 9a, is applied to the CRGA internal components. This PSD is shown in Figure 4-50 and described in detail in Section 4.5.1.1.4.

Typically, this PSD is considered appropriate for tubes in heat exchangers with diameters in the range of ~ ½ to ¾ inches with pitch-to-diameter ratios of approximately 1.4. The c-tubes, tie rods, and RCCA fit this criteria. The PSD has equivalency in this aspect. For the excitation resulting from the cross flow conditions, a correlation length [ ] is applied to all spans.

Table 4-21—Thermal-Hydraulic Inputs for the CRGA and the RCCA

[ ]

Note(s) for Table 4-21:

1. Refer to Figure 4-60 for the locations along the length of the CRGA at which these thermal hydraulic conditions are applied.
2. This table shows a maximum axial velocity of 0.31 ft/sec considering either the upward or downward flow through the CRGTs. A conservative cross flow velocity of 0.31 ft/sec is applied to the components in the upper spans of the CRGA for the RTE analysis, as shown in Figure 4-60.
3. The lower spans of the CRGA are hydraulically open and subject to the thermal hydraulic conditions in the upper plenum. This table shows a velocity of 4.7 ft/sec for the RCCA interior locations of the CRGA in the lower spans, which is less than the cross flow velocity for the peripheral location of the lower spans (e.g., 13.9 ft/sec and 9.4 ft/sec). A cross flow velocity of 4.7 ft/sec is conservatively applied to the RCCA in the upper spans of the CRGA for the VSE analysis.

Figure 4-39—Control Rod Guide Assembly (CRGA)

[

]

4.6.4 FIV Acceptance Criteria for the CRGA Components

4.6.4.1 Random Turbulence-Induced Vibration

The turbulence-induced vibration analysis is based on Powell's joint acceptance technique (Reference 8), which computes only the RMS vibration amplitude and stresses. The displacements are computed in units of (inch, rms), the moments in units of (in-lbs, rms) and the reaction loads at support locations in units of (lbs, rms).

Acceptance Criteria for Displacements

To verify that the tie rods, the c-tube, and the control rod assembly do not impact each other, the displacements are conservatively limited to one-half the minimum distance between these adjacent structures. Because the computed displacement response to turbulence is based on a probability of excursions, the displacements (determined in units of inch, rms) are multiplied by a factor of five or five sigma, which represents approximately 100 percent probability that the computed displacement will not be exceeded.

The allowable displacement limit is based on the minimum clearance between each of the three components considering the centerline distance of [ ] inches between the centerline of the tie rod and the (c-tube and/or RCCA) and the OD of the tie rod ([ ] inch) and the OD of the c-tube ([ ] inch) to provide a minimum clearance of [ ] inch. Considering a five sigma value of probabilities of vibration amplitudes for each structure, this value is reduced by a factor of 10 to provide the acceptable displacement limit of [ ] inch, rms for the tie rods, c-tubes and RCCA.

For the interfacing location of the RCCA and the c-tubes in the continuous region of the CRGA, interaction between these two components is inevitable. The MAGALY testing program took measures to optimize the interaction between these two components to limit the wear and vibrations. An allowable displacement limit is not established for these two structures in the CRGA.

Acceptance Criteria for High Cycle Fatigue

The criterion established in Section 4.2.6.2 using fatigue curve “B” is applied to the CRGA internal components. The mean stress in the components of the CRGA is less than 27.2 ksi, but the stress location may be within three wall thicknesses of the centerline of a weld. The allowable stress for fatigue curve “B” is [ ] psi, rms at 10^{13} cycles. This allowable stress is adjusted to account for differences in the modulus of elasticity of the CRGA materials to provide an allowable stress of [ ] psi, rms at 10^{13} cycles.

4.6.4.2 Vortex-Shedding Induced Vibration

Acceptance Criteria for Displacements

The acceptance criterion for the off-resonant response of the CRGA internal is identical to that established for random turbulence with the exception of the units. Because the response to vortex-shedding is harmonic, the allowable displacement and the allowable stress are in units of 0-peak. As computed for turbulence, the allowable displacement limit of [ ] inch, (0-peak) is applied to the tie rods, the c-tube and RCCA.

Acceptance Criteria for High Cycle Fatigue

The ASME fatigue curve "B" shown in Figure 4-21 is applied for the off-lock in response of the austenitic stainless steel components of the CRGA. The allowable high cycle fatigue stress of [ ] psi (0-peak) is at 10^{11} cycles for fatigue curve "B."

4.6.5 Response of the CRGA Components

The CRGA tie rods, the c-tubes, and the RCCA control rod assemblies are not susceptible to vortex lock-in conditions because this mechanism is either avoided or suppressed based on the results and acceptance criteria shown in Table 4-22 through Table 4-24. Figure 4-61 through Figure 4-65 provide the frequency and mode shape plots for these CRGA components. Figure 4-66 through Figure 4-71 provide the displacement response PSD for these CRGA components. The vortex-shedding frequencies for these components are well separated from the modal frequencies. The response to this type of flow excitation, if occurring, can be considered quasi-static and no further evaluation is required.

The results of the full scale analysis for random turbulence shown in Table 4-25 demonstrates that the CRGA tie rods, c-tubes, and the RCCA are not susceptible to high cycle fatigue failure. The results show that the tie rods, c-tubes, and the RCCA do not impact each other or result in failure caused by impact.

A comparison of the modal frequencies for the c-tubes and the RCCA confirms that conditions do not exist between these components that would lead to resonant excitation during contact with each other. The fundamental modal frequencies are separated by more than [ ] Hz and therefore, the c-tube can not be mechanically excited by the RCCA.

Table 4-22—Susceptibility of CRGA Tie Rod to Vortex-Shedding Lock-In

[ ]

Table 4-23—Susceptibility of CRGA C-Tube to Vortex-Shedding Lock-In

[ ]

Notes for Table 4-22 and Table 4-23:

1. Both criteria (a) and (d) are met and vortex lock-in does not occur for the CRGA tie rods or the c-tubes. Because the shedding frequencies and the modal frequencies are well separated, the response is quasi-static and the computation of the off lock-in forced vibration response is not required.

Table 4-24—Susceptibility of RCCA to Vortex-Shedding Lock-In

[ ]

Table 4-25—CRGA FIV Results for Random Turbulence Excitation

[ ]

Notes for Table 4-25:

1. A FSRF of 5.0 is applied to the stresses in this table.

4.6.6 Conclusions

The FIV analysis is performed for thermal-hydraulic conditions with four RCPs operating. Based on the large margins for displacements and stresses for the CRGA and RCCA structures computed for the full power normal operating conditions, there is ample margin for these structures during other RV transient conditions as follows:

- Ten percent RCP overspeed transient conditions that may occur during full power normal during operating conditions.
- Different combinations of RCP operation (i.e., one, two, or three RCP combinations).

Explicit analytical evaluations of the short term transients are not performed. These transient conditions are evaluated as follows:

Because a 10 percent RCP overspeed transient condition produces a [ ] percent increase in the primary flow through the RV internals, a [ ] percent increase in the flow through the CRGAs is expected. This increased flow rate creates a [ ] percent increase in the response of the CRGA and RCCA structures or a scaling factor of [ ] based on the relationship for the dynamic pressure term. Applying this scaling factor to the results reported in Section 4.6.5 for full power normal operating conditions and the allowable FIV limits justifies the 10 percent RCP overspeed transient.

The high cycle fatigue imparted to the CRGA and RCCS structures as a response to turbulence resulting from the transients associated with one, two, or three RCP operation is insignificant for the reasons identified in Section 4.5.4 for the column supports in the RV upper internals.

4.7 Heavy Reflector Tie Rods

4.7.1 Description of Tests for the Tie Rod

The HR slabs are held together by [ ] tie rods (See Figure 4-26). Full-scale tests are carried out to assess the vibratory behavior of the HR tie rods which experience axial flow conditions.

The tie rods are long tubes with a [ ] inch outer diameter and [ ] inch inner diameter. The main function of the tie rods is to enable handling of the HR during removal of the lower internals. The tie rods are not integral to the design or function in any aspect relative to the vibratory behavior of the HR. They do not serve to prevent or inhibit flow induced vibrations of the HR slabs. However, the tie rods experience the cyclic loading created by interaction with the HR and the response of the flexural modes of the HR to random turbulence and Poisson's effect. The justification that the tie rods will not fail from the effects of high cycle fatigue created by this load source and excitation is provided in Section 4.7.3.

The tie rods are cooled by flow through an annulus in the HR between the bottom and top HR slabs. The cross sectional flow area of the annulus is reduced at slab interfaces by centering rings. The mock-up test for the tie rod represents the tie rod and its environment (slabs and centering rings) at full scale. The tie rod is equipped with strain gauges at its ends to allow adjustment of the preload and to characterize the embedment conditions. The tie rod is also equipped with six accelerometers regularly spaced over the length.

The test program is divided into three steps:

- In-air frequency test and modal analysis: The natural frequencies, damping ratios, and mode shapes are measured for various magnitudes of the preload.
- Still-water frequency test and modal analysis: The natural frequencies, damping ratios, and mode shapes are measured for various magnitudes of the preload.
- Flow tests: Vibratory response when subjected to flow.

The flow tests are performed under the following conditions:

- Two preload values of [ ] lbs (≈ nominal preload) and [ ] lbs (representative of the eventual stress relaxation).
- Flow rate between [ ] ft^3/min (≈ twice the design flow rate). This maximum flow rate provides a nominal velocity of approximately [ ] /sec through the annulus of the HR.

These tests are performed at room temperature.

The primary purpose of the flow test is to assess if fluid-structure coupling between the tie rod and the fluid flow the annulus in the HR occurs. The expected tie-rod behavior to varying flow rates is as follows:

At low flow rates, the random vibration amplitudes of the tie rod are small. With increasing flow rates, the parallel flow excitation of the fundamental mode is increased and becomes maximized when the phase relationship between this mode and the convective velocity (U_c) becomes coincident, increasing the coherence of the forcing function. Under these flow conditions, the vibration amplitudes of the tie rod reach a peak. For higher flow rates, it is possible that fluid-structure coupling may occur, leading to axial flow instability of the tie rod.

4.7.2 Results of the Flow Test for the Tie Rods

The modal frequencies of the tie rod under various preloads are summarized in Table 4-26 and the mode shapes are shown in Figure 4-41 and Figure 4-42. The mode shapes and frequencies of the tie rods are consistent with calculations based on beam theory. The damping ratio is reported in Table 4-27 for values of preload and shows that the damping ratio increases with decreasing preload for both of the environments tested. The measurements for the damping ratio are determined using the following expression:

$$\zeta = \frac{1}{2\pi n}\log_e\left(\frac{y_i}{y_{i+n}}\right)$$

The purpose of the flow tests is to determine if fluid-structure coupling occurs between the tie rod and the flow conditions in the annulus of the HR. Such phenomena are more susceptible at a low level of preload as this leads to lower natural frequencies of the tie rod. For the target preload value of [ ] lbs, the tie rod does not show any evidence of random turbulence induced by parallel flow excitation or any evidence of fluid structure coupling. After decreasing the preload directly to the most penalizing preload value of [ ] lbs, neither random vibration nor fluid structure coupling is observed at the maximum flow rate and the interaction between the tie-rod and fluid flow is limited.

The maximum flow rate for the test is approximately twice the design. At the design flow rate (nominal velocity = [ ] ft /sec), the tie rod is not susceptible to significant turbulent excitation due to parallel flows, even at the lower values of preload. This flow rate is below the critical velocity that would lead to fluid-structure coupling or axial fluid instability of the tie rod.

4.7.3 Cyclic Loading of Tie Rods Created by Response of Heavy Reflector to Random Turbulence

As reported in Section 4.7.2, the tie rods are not susceptible to significant flow excitation created by the parallel flow through the annulus in the HR. However, the tie rods experience cyclic loading created by interaction with the HR and the response of the flexural modes of the HR to random turbulence. The justification that the tie rods will not fail from the effects of high cycle fatigue that is created by their interaction with the HR is provided in this section.

Full scale testing of the tie rods is performed to determine the resonant response for the first two modes of the tie rod when subjected to various levels of excitation or amplitudes of vibration. The excitation of the tie rod is performed by means of an electrodynamic exciter with the capability to scan frequencies such that resonant excitation of the tie rod is accomplished for a range of preloads. The preload in the tie rod is measured with strain gages located near the ends of the tie rod. The accelerations along the length of the tie rod that are experienced as a result of various amplitudes of resonant excitation induced to the tie rod is determined with the six accelerometers positioned on the tie rod as depicted in Figure 4-26. These accelerations are then converted to a magnitude of stress in the tie rod which is reported in Table 4-35 and Table 4-36 respectively for both the in-air and in-water test.

As shown in Table 4-36 for the first mode, a maximum stress of [ ] psi and an amplitude of displacement equal to [ ] inches was measured in the tie rod for the most limiting in-water test. The result from this test is representative of the resonant excitation of the tie rod at its first natural frequency of 7.7 Hz consistent with a preload of 11,688 lbs. Considering a stress concentration factor of 4, the peak stress would be [ ] psi.

The fatigue curves (curve a) published in the 2004 edition of the ASME Section III, Appendix I, Table I-9.2.2 or Figure 4-21 has an endurance limit of 23,700 psi at 10^{11} cycles. This endurance limit allows for approximately [ ] inches [ ] of vibrational amplitude in the tie rod for the cold condition and a little less than this value for the hot conditions.

The predicted amplitude of vibration for the response of the HR beam mode at its mid-span elevation or location HR_A1 is [ ] inches ([ ] Hz) as reported Table 4-10. The comparison of this displacement to the endurance limit of [ ] inches for the tie rod, demonstrates that it is not possible for the tie rod to fail from the worst case scenario of resonant excitation created between the response of the flexural modes of the HR to turbulence and the first mode of the tie rod. It is noted that this justification assumes that the cyclic loads or strains are induced on the tie rods. Since the tie rods and the twelve slabs of the HR behave as clamped members, the tie rods are relatively immune to the axial strains that the HR experiences which, as stated above, are created by the flexure of both the shell and beam modes of the HR and Poisson's effect. Since the mating surfaces of the HR slabs do not separate, the additional axial load that is created by the inertia effects of the HR, beyond that of the preload, is not induced on the tie rods.

4.7.4 Conclusions

The tests conclude that:

- The registered natural frequencies are consistent with the theoretical approach.
- High damping ratios exist, particularly in water.

No tie rod vibration is detected even for the worst case test conditions of a lower preload value and the maximum test flow rate (or twice the design flow rate). The risk of fluid-structure coupling phenomena does not exist. Further, it is not possible for the tie rods to fail from the effects of high cycle fatigue that is created by interaction with the HR and the response of the flexural modes of the HR to turbulence.

Table 4-26—Modal Frequencies of the HR Tie Rods

[ ]

Table 4-27—Damping Coefficients for the HR Tie Rods

[ ]

Figure 4-40—Heavy Reflector Tie Rods

Table 4-28—List of Sensors Used with the HYDRAVIB Mockup Testing

Sensor Reference	Sensor Type	Individual Tests					Tests on Assembled Components		
		CB Static Tests	FDD Static Tests	CB Modal Analysis	HR Modal Analysis	FDD Modal Analysis	Modal Analysis	Flow Test	Forcing Function
Kistler 9321 A	force sensor			X	X	X			
Bruel & Kjaer 4374	accelerometer			X	X	X			
Kistler 9321B	force sensor						X		
Bruel & Kjaer 4375W01	accelerometer						X		
PCB 352C68	accelerometer						X		
TME HS 10	displacement		X						
KYOWA KFG1-120-C1	strain gauge		X						
KYOWA KFG10-120-C1	strain gauge		X						
KAMAN 5CM-KD2440	displacement	X						X	
DJB A/23/TS	accelerometer							X	
PCB 352C65	accelerometer							X	
PCB 352C66	accelerometer							X	
PCB 352C68	accelerometer							X	
VIBROMETER TQ401	displacement							X	
PCB 112A21	dynamic pressure							X	X
PCB 113A21	dynamic pressure								X
PCB WM105C02	dynamic pressure							X	X
VISHAY CEA 06-062UW-350	strain gauge							X	
VISHAY LWK-06-W250B-350	strain gauge							X	
KYOWA SKW - 10642	strain gauge							X	

Table 4-29—Characteristic of the Sensors used with HYDRAVIB Mockup Testing

Sensor Reference	Sensor Type	Sensor Characteristics - SI Units		
		Amplitude Range	**Frequency Range**	**Linearity**
KAMAN 5CM-KD2440	displacement	0-2.9 mm	DC to 10 kHz	N/A
DJB A/23/TS	accelerometer	49050 m/s^2 pk	10 Hz to 4 kHz	N/A
PCB 352C65	accelerometer	491 m/s^2 pk	0.5 Hz to 10 kHz	5% or better
PCB 352C66	accelerometer			
PCB 352C68	accelerometer			
VIBROMETER TQ401	displacement	0-2.0 mm	DC TO 20 kHz	3dB or better
PCB 112A21	dynamic pressure	0 to 690 kPa	0.5 Hz to 100 kHz	5% or better
PCB 113A21	dynamic pressure	0 to 1380 kPa	0.5 Hz to 100 kHz	5% or better
PCB WM105C02	dynamic pressure	0 to 690 kPa	0.5 Hz to 100 kHz	5% or better
VISHAY CEA 06-062UW-350	strain guage	N/A	N/A	N/A
VISHAY LWK-06-W250B-350	strain guage	N/A	N/A	N/A
KYOWA SKW-10642	strain guage	N/A	N/A	N/A

Table 4-30—U.S. EPR RCP Shaft and Blade Passing Frequencies (Design)

[ ]

Note(s) for Table 4-30:

1. The wave lengths in this table are based upon a sonic velocity of 2902 ft/sec consistent with the full power normal operating conditions.

Table 4-31—Static Forces Acting on the Support Columns

[ ]

Table 4-32—Comparison of Natural & Vortex-Shedding Frequencies for the Column Supports

[ ]

Table 4-33—Dynamic Amplification Factors for the RCP Acoustic Pressure Fluctuations

Table 4-34—Reduced Damping for the CRGA Control Rod Absorber (Viscous)

[ ]

Notes:

1. The viscous fluid damping is determined from the following relationship taken from Reference 2, Equation 8-23:

$$\zeta_{fluid} = C_{lift}\left(\frac{1}{8\pi}\right)\left(\frac{V}{f \cdot D}\right)\left(\frac{\rho \cdot D^2}{m_t}\right)$$

2. $\zeta(hysteresis)$ is the damping of the material resulting from hysteresis.
3. $\zeta(structural)$ is the damping created by the non-linear interaction of the control rod absorber and the guide plates.
4. The reduced damping (C_n) is determined from the relationship in ASME Code Section III, Appendix N-1324.1.

Table 4-35—Stress Results for Resonant Excitation of the HR Tie Rods (In-Air)

Table 4-36—Stress Results for Resonant Excitation of the HR Tie Rods (In-Water)

Table 4-37—Vibration Amplitude of LSP for Various Combinations of Pump Operation (from HYDRAVIB Mockup)

Figure 4-41—HR Tie Rod Mode Shape in Still Water (Mode 1)

Figure 4-42—HR Tie Rod Mode Shape in Still Water (Mode 2)

Figure 4-43—HYDRAVIB Instrumentation for Static Testing of Core Barrel

Figure 4-44—HYDRAVIB Instrumentation for Static Testing of Flow Distribution Device

[ ]

Figure 4-45—HYDRAVIB Instrumentation for Modal Testing of Core Barrel

Figure 4-46—HYDRAVIB Instrumentation for Modal Testing of Heavy Reflector

[ ]

Figure 4-47—HYDRAVIB Instrumentation for Modal Testing of Flow Distribution Device

Figure 4-48—HYDRAVIB Instrumentation for Modal Testing of Core Barrel Assembly (Core Barrel Instrumentation)

Figure 4-49—HYDRAVIB Instrumentation for Modal Testing of Core Barrel Assembly (Heavy Reflector Instrumentation)

Figure 4-50—Random Lift Coefficient for U.S. EPR Upper Internals

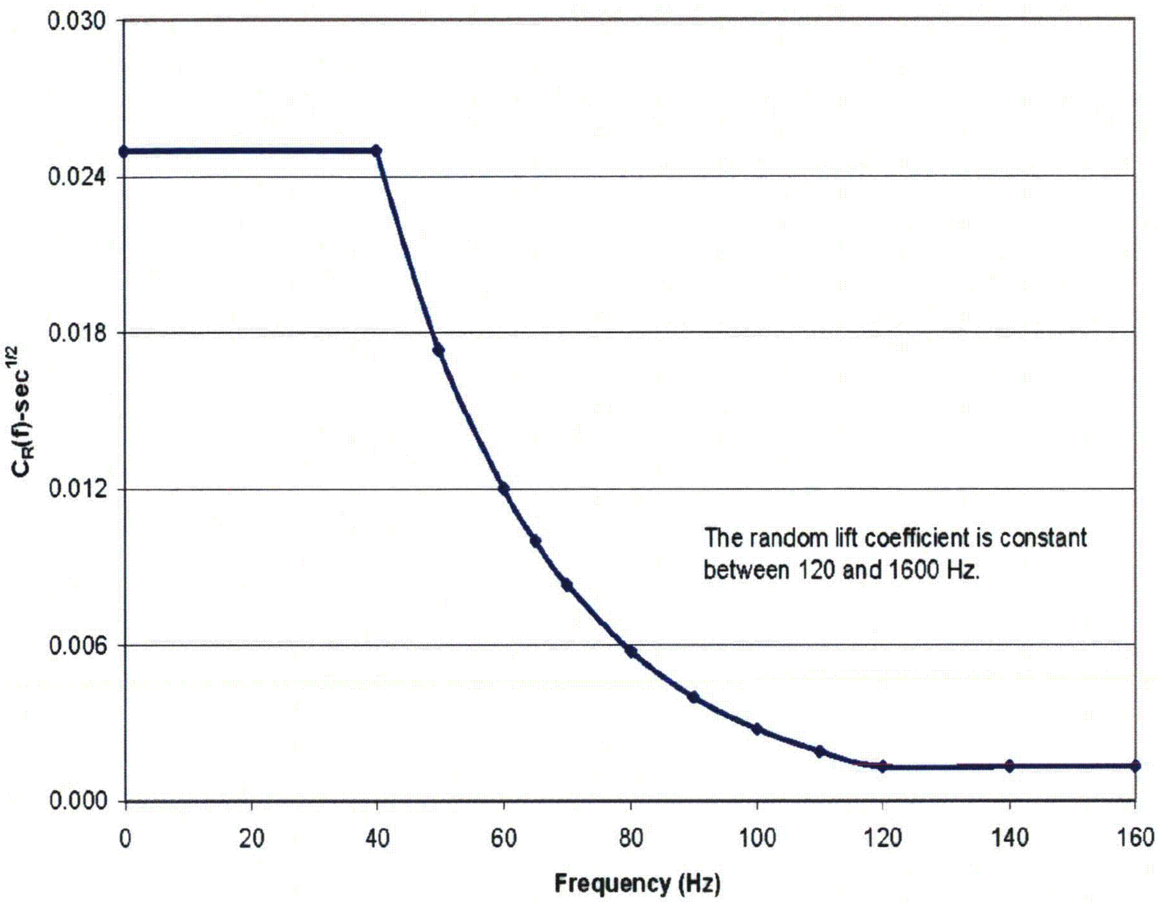

Figure 4-51—Mode Shapes for the Normal Support Column (axial load = -4500 lbs)

Figure 4-52—Mode Shapes for the LMP Support Column (axial load = -3600 lbs)

Figure 4-53—Mode Shapes for the CRGA Support Column (axial load = -7500 lbs)

[ ]

Figure 4-54—Mode Shapes for the Instrumentation Guide Tube

[ ]

Figure 4-55—Displacement Response PSD for Normal Support Column

[ ]

Figure 4-56—Displacement Response PSD for LMP Support Column

[ ]

Figure 4-57—Displacement Response PSD for CRGA Support Column

Figure 4-58—Displacement Response PSD for Instrumentation Guide Tube

Figure 4-59—Acoustic Wave Impinging Normally on a Cylinder

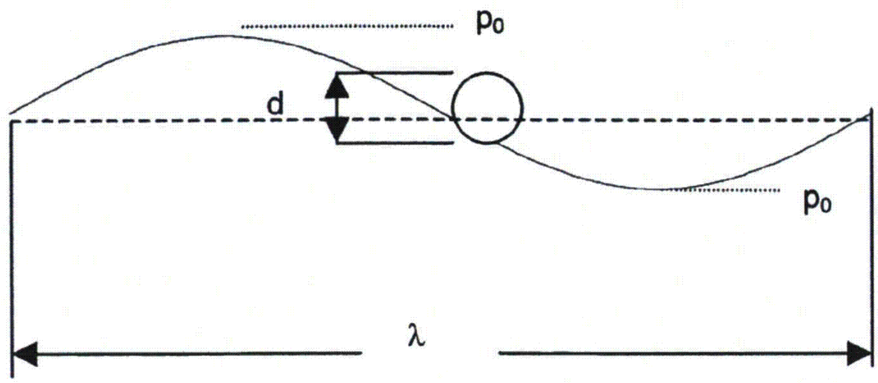

Figure 4-60—CRGA and CRGA Column Support

Note(s) for Figure 4-60:

1. The RCCA is not depicted with this figure but it is evaluated for RTE considering the cross flow velocity shown in this figure. For the analysis of VSE, the interior locations of the control rods not protected by the c-tubes consider a 4.7 ft/sec cross flow velocity in both the lower and upper spans of the CRGA.

**Figure 4-61—CRGA Tie Rod Frequencies and Mode Shapes
Sheet 1 of 2**

[ ]

Figure 4-61—CRGA Tie Rod Frequencies and Mode Shapes
Sheet 2 of 2

[ ]

Figure 4-62—CRGA C-Tube Frequencies and Mode Shapes (in-plane)
Sheet 1 of 2

Figure 4-62—CRGA C-Tube Frequencies and Mode Shapes (in-plane)
Sheet 2 of 2

[ ]

**Figure 4-63—CRGA C-Tube Frequencies and Mode Shapes (out-of-plane)
Sheet 1 of 2**

**Figure 4-63—CRGA C-Tube Frequencies and Mode Shapes (out-of-plane)
Sheet 2 of 2**

[ ]

Figure 4-64—CRGA RCCA Frequencies and Mode Shapes (in-plane)
Sheet 1 of 3

**Figure 4-64—CRGA RCCA Frequencies and Mode Shapes (in-plane)
Sheet 2 of 3**

[

]

Figure 4-64—CRGA RCCA Frequencies and Mode Shapes (in-plane)
Sheet 3 of 3

[ ]

**Figure 4-65—CRGA RCCA Frequencies and Mode Shapes (out-of-plane)
Sheet 1 of 3**

[ ]

Figure 4-65—CRGA RCCA Frequencies and Mode Shapes (out-of-plane)
Sheet 2 of 3

**Figure 4-65—CRGA RCCA Frequencies and Mode Shapes (out-of-plane)
Sheet 3 of 3**

[ ]

Figure 4-66—CRGA Tie Rod Displacement Response PSD

[ ]

Figure 4-67—CRGA C-Tube Displacement Response PSD (in-plane)

[ ]

Figure 4-68—CRGA C-Tube Displacement Response PSD (out-of-plane)

[ ]

Figure 4-69—CRGA RCCA Displacement Response PSD (in-plane) (Between Bottom Flange/Guide Plate and Bottom End of RCCA)

Figure 4-70—CRGA RCCA Displacement Response PSD (in-plane)
(Between 5th Intermediate Guide Plate and Bottom Flange/Guide Plate)

[ ]

**Figure 4-71—CRGA RCCA Displacement Response PSD (in-plane)
(Between RCCA Spider and 5th Intermediate Guide Plate)**

Figure 4-72—U.S. EPR CFD Model

[ ]

5.0 VIBRATION AND STRESS MEASUREMENT PROGRAM

In accordance with Reference 1, a vibration and stress measurement program is developed for the U.S. EPR RV internals. The purpose of the measurement program is to verify the structural integrity of the reactor internals, determine the margin of safety associated with steady state and anticipated transient conditions for normal operation, and to confirm the results of the vibration analysis.

5.1 Objectives

The pre-operational tests described in this section include measurements of the vibratory response of the RV internals for various primary flow rate conditions. The tests are performed with the following objectives:

- To provide information that enables a direct assessment of the RV internals vibratory behavior.
- To verify analysis methods.
- To provide reference data for the adjustment of the numerical models for the final compressive vibration assessment report.
- To provide reference data for the VMS calibration.

5.2 Instrumentation

5.2.1 Permanent Instrumentation

The permanent instrumentation corresponds to the VMS sensors attached to the outside of the RV and is composed of four absolute displacement transducers implemented on the RV head at 0, 90, 180 and 270 degree orientations (See Figure 5-1 and Figure 5-2). These displacement sensors directly measure vibration of the RV. The VMS also includes eight excore detectors, four upper and lower pairs located at 45, 135, 225 and 315 degrees. (See Figure A-3.) The excore neutron flux signal is stripped of its static neutron flux and the fluctuations are monitored to infer motions of the CB, HR, and the FAs.

The vibration characteristic functions are determined by Fast-Fourier-Transformation of the measured signals in the time domain into the frequency domain (auto-spectra, cross-spectra, coherence functions, transfer functions magnitude, and phase). In these functions, the vibration characteristics of the monitored components appear as magnitude peaks. Therefore, changes in these peaks during the life of the component can be directly attributed to changes in the component's vibration behavior.

The VMS also includes other sensors attached to the RCS piping and the main steam and feedwater line piping systems as identified in Appendix A and Figure A-2. The discussions provided in this chapter are limited to the sensors that can be used to characterize the RV internal vibrations.

5.2.2 Temporary Instrumentation

The temporary instrumentation includes:

- Displacement sensors.
- Strain gauges.
- Accelerometers.
- Dynamic pressure transducers.

The sensor type is chosen for the expected range of vibration frequencies. Table 5-1 to Table 5-3 and Figure 5-1 to Figure 5-13 identify the instrumentation.

5.2.2.1 Instrumentation for RV Lower Head

The temporary instrumentation installed on the outside of the RV is composed of two displacements sensors implemented at the RV bottom (See Table 5-1, Figure 5-1, and Figure 5-3). The objective is to characterize the pendulum mode response of the RV and the potential quasi-static motions (at low frequency).

5.2.2.2 Instrumentation of the RV Lower Internals

The experience feedback from existing AREVA NP units and the HYDRAVIB tests shows that the lower internals mainly respond at very low frequencies (quasi-static response to the pressure fluctuations in the downcomer) and to the beam mode. The characterization of this response is the main objective of the pre-operational tests and redundancy is established with the instrumentation of the RV lower internals. This instrumentation includes:

- Three groups of dynamic pressure transducers flush mounted on the CB to measure the pressure fluctuations in the downcomer. Each group or array of dynamic pressure transducers consists of five sensors arranged in a cross pattern with a maximum separation of 2.0 inches.
- Two displacement sensors between the LSP and the RV keys (if not feasible, these two sensors will be replaced by accelerometers with low frequency sensitivity).
- Two horizontal accelerometers on the LSP.
- Four strain gauges near the CB flange. These strain gauges are a backup instrumentation in case of loss of the previous accelerometers and displacement sensors.

See Table 5-2, Figure 5-1, Figure 5-4, and Figure 5-5 for additional information regarding the type and location of the sensors.

The instrumentation of the lower internals is completed by measurements at the top HR slab and is implemented to characterize potential low frequency motions between the HR and the CB and to characterize the shell mode response of these two components. This instrumentation is composed of::

- Four relative displacement sensors with a 45° spacing between the HR and the CB, at the HR top.
- Four radial accelerometers with a 45° spacing mounted on the CB.

See Figure 5-6 for additional information regarding the type and location of the sensors.

Note the 45° spacing is retained because the HR shape leads to non axis-symmetric modes.

The risk of significant vibration is not expected for the FDD because of its high natural frequencies. The HYDRAVIB tests confirm this assessment. Nevertheless, the FDD is instrumented because it is a new design. The instrumentation of the FDD is composed of:

- Two radial accelerometers with a 45° spacing mounted on the FDD shell.
- One vertical accelerometer at the FDD center.

See Figure 5-7 for additional information regarding the type and location of the sensors.

Note the 45° spacing is retained because the FDD has axis-symmetric "shell" modes. Because the VMS is more sensitive to the detection of the vertical modes, only two or three vertical accelerometers are implemented on the LSP (See Figure 5-4 and Figure 5-5).

5.2.2.3 Instrumentation for the RV Upper Internals

The experience feedback from the existing AREVA NP units does not show significant overall vibrations of the upper internal assembly. The characteristic "beam" natural frequency for this assembly is too high to be strongly excited by turbulent flows. The U.S. EPR upper internals are stiffer than previous ones and therefore, no deviation in this experience is expected for the U.S. EPR RV internals. In order to confirm this assessment, four horizontal accelerometers are implemented on the UCP (See Figure 5-8 and Figure 5-9). Because the VMS is more sensitive to vertical modes, either two or three vertical accelerometers are implemented on the USP.

The main objective of the instrumentation of the upper internals is to characterize behavior of the columns and CRGAs. The CRGA column at location S6 (or a symmetric one) and the LMP column at location T7 (or a symmetric one) are chosen because these columns are exposed to the most transverse flows (See Figure 5-10). These two columns are instrumented with four vertical strain gauges near the top flange (See Figure 5-8, Figure 5-12, and Figure 5-13). Only two gauges are strictly needed per column, while the other two provide a redundancy of measurements.

The CRGAs are protected against the flows in the plenum by the CRGA columns, and the MAGALY tests have shown that the flows exiting the bottom of the column do not induce significant vibration of the CRGA. As the first natural frequency of the CRGAs is about [ ] Hz, the CRGAs should follow the quasi-static general motions of the upper internals. In order to confirm these assessments, two CRGAs are instrumented (See Figure 5-10):

- The central location of J9.
- The peripheral location if S6 (or symmetric one).

Each location is equipped with two radial accelerometers at mid-height (See Figure 5-11).

Table 5-1—Instrumentation of the RV for Pre-operational Tests

Component	Transducers			Frequency range			Measurements	Observations
	Identification	Number of channels	Type	Static	< 5Hz	> 5Hz		
Vessel head	VMS1 to VMS4	4	Absolute displacements		×	×	RV pendulum mode and quasi-static motions. Detection of RV internal "beam" and vertical modes.	VMS sensors
Vessel bottom	RVB0 and RVB90	2	Absolute displacements		×	×	RV pendulum mode and quasi-static motions	
Total number of channels		6						

Table 5-2—Instrumentation of the Lower Internals for Pre-operational Tests

Component	Transducers			Frequency range			Measurements	Observations
	Identification	# of channels	Type	Static	< 5Hz	> 5Hz		
Lower support plate	LSP_{V1} and LSP_{V2} (LSP_{V3} if possible)	2 (or 3)	Accelerometers			×	LSP vertical mode	For VMS calibration
	LSP_{R1} - LSP_{T1} LSP_{R2} - LSP_{T2}	4	4 Accelerometers or 2 accelerometers + 2 displacement sensors		×	×	RV internal beam modes and quasi-static motions	
Core barrel and heavy reflector	CB_{P1}, CB_{P2}, CB_{P3}	15	3 arrays of (5) dynamic pressure sensors		×	×	Dynamic pressure measurements between inlet nozzles and middle region of CB	
	CB_0 to CB_{135}	4	Accelerometers and / or		×	×	Core barrel shell modes	
	HR_0 to HR_{135}	4 (base)	displacement sensors		×	×	Heavy reflector "shell" modes and quasi-static motions	
Core barrel flange	CBF1 to CBF4	4	Strain gauges		×	×	RV internal beam mode and quasi-static motions	
Flow distribution device	FDD_{R0} and FDD_{R45}	2	Accelerometers			×	FDD beam and shell modes	
	FDD_V	1	Accelerometer			×	FDD "plate" mode	
Total number of channels		36 (37)						

Table 5-3—Instrumentation of Upper Internals for Pre-operational Tests

Component	Transducers			Frequency range			Measurements	Observations
	Identification	# of channels	Type	Static	< 5Hz	> 5Hz		
Upper support plate	USP_{V1} and USP_{V2} (USP_{V3} if possible)	2 (or 3)	Accelerometers			×	Upper internals vertical mode	For VMS calibration
Upper core plate	UCP_{R1} - UCP_{T1} UCP_{R2} - UCP_{T2}	4	Accelerometers			×	Upper internals beam modes	
CRGA (locations S6 and J9)	$CRGA_1$ to $CRGA_4$	4	Accelerometers			×	CRGA bending modes at locations J9 and S6	
CRGA columns (location S6)	SC_1 to SC_4	4	Strain gauges	×		×	Static bending and bending modes of column	
LMP columns (location T7)	LMP_1 to LMP_4	4	Strain gauges	×		×	Static bending and bending modes of column	
Total number of channels		18 (19)						

Figure 5-1—Pre-operational Test Instrumentation - Overview

Figure 5-2—VMS Permanent Instrumentation

Figure 5-3—RV Bottom Head Instrumentation

Figure 5-4—Lower Internals Instrumentation

Figure 5-5—Lower Support Plate Instrumentation

Figure 5-6—Core Barrel and Heavy Reflector - Instrumentation

Notes for Figure 5-6:

1. Transducers: accelerometers or relative displacement sensors.

Figure 5-7—FDD Instrumentation

Figure 5-8—Upper Internals - Instrumentation

Figure 5-9—Upper Core Plate Instrumentation

[

]

Figure 5-10—Instrumented Locations of CRGA, CRGA Column and LMP Column

[ ]

Figure 5-11—CRGA Guide Plate Instrumentation

[ ]

Figure 5-12—CRGA Column Instrumentation

Figure 5-13—LMP Column Instrumentation

5.3 Test Conditions

The objectives of the pre-operational and the initial start tests are:

- To characterize the vibratory behavior of the RV internals in steady state flow conditions and in expected transient conditions.
- To provide a means to verify and adjust, if necessary, the theoretical predictions of the behavior of the RV internals developed in the vibration and stress analysis program (Section 4.0).

The tests that are planned for the pre-operational and the initial startup phases are outlined in the following sections.

5.3.1 Pre-Operational Tests

Considering that the vibratory behavior of the RV internals is primarily a function of the flows and that only large scale temperature transients could influence the vibratory response through evolutions of the physical characteristics of the primary fluid, the following relevant transients are tested:

- Plant heatup and cooldown.
- Main coolant pumps startup or stop (one pump or more simultaneously).

The plant heatup and cooldown transients are sufficiently slow to be assumed as a succession of steady state flow conditions. Consequently, the relevant steady state conditions are the following:

- Operation with the four main coolant pumps at several temperature levels from cold to hot conditions.
- Operation with less than four main coolant pumps in cold and hot conditions.

Various conditions are tested in order to cover the potential situations. Table 5-4 presents the test program. The total duration of the tests verifies that the total accumulation of vibration cycles is greater than 10^6 based on the frequency of the pendulum mode of the lower internal assembly (~ **[ ]** Hz). The use of dummy fuel assemblies or an alternate flow restrictor during HFT to assess the integrity of the RPV internals to flow induced vibration is not required although, the use of these devices may be necessary in order to accomplish the objectives of other tests performed for other systems during the HFT program which are outside the scope of this comprehensive vibration assessment program. The justification that the use of the dummy FAs or an alternate flow restrictor is not essential to the verification of the structural integrity of the RPV internals for flow-induced vibration during the test identified in Table 5-4 is provided in Section 4.2.5.1.3.

5.3.2 Initial Startup Tests and Full Power Tests

The initial startup tests and full power tests are performed with only the VMS instrumentation to finalize the VMS calibration and to make a final validation of the overall model of the RV internals. Considering these objectives, the tests are carried out in steady states conditions.

Table 5-4—Pre-Operational Test Program

Test number	Configuration	Characteristics	
		Temperature	Pressure
1	1 pump	140°F	390 psia
2, 3, 4	2 pumps : 3 cases		
5	3 pumps		
6	4 pumps		
7	Transient 4/0 pump		
8	1 pump	250°F	390 psia
9	4 pumps		
10	1 pump	400°F	1015 psia
11	4 pumps		
12	1 pump	578°F	2250 psia
13, 14, 15	2 pumps		
16	3 pumps		
17	4 pumps		
18	Transient 4/0 pump		

5.4 Acquisition of Test Data

5.4.1 Precautions to Ensure Quality of Data

All transducers are selected to perform in the anticipated environment. Transducers are calibrated per the AREVA NP QA program.

A frequency band width between 0 Hz to 250 Hz, which covers the second blade passing frequency of the RCP, is required for vibration assessment. Based on the upper frequency limit of the data being equal to one-half the sampling rate, a minimum sampling rate of 500 Hz is required to capture this range of frequencies. However, a sampling rate of at least 5 kHz is used to verify the accuracy of the amplitude and not just the resolution of the Nyquist frequency. The time history data blocks are a sufficient duration of time to verify that the sampling rate does not compromise a resolution of 0.1 Hz in the frequency when converted with the FFT to obtain the PSDs.

The PSDs are calculated by block averaging methods using a Hanning window to provide the statistical accuracy. For steady state conditions, a minimum of 100 blocks are averaged. A sample rate of 5 kHz yields a 0 to 2.5 kHz PSD with usable data to 2 kHz . The number of points in the PSD is half the number of samples in each block. To achieve a frequency resolution of 0.1 Hz with a 5k sample rate, the block must be 50K data points in length or ten seconds. Considering 100 blocks, each with 10 seconds of time duration, each PSD will require 16 minutes and 40 seconds of data acquisition. A minimum of 20 minutes are recorded for steady state conditions

5.4.2 Data Acquisition System

The data recording system is designed to record the time history digital data from the transducers on personal computer storage devices. The instrumentation cables directed out of the RV are terminated at a junction box. The signals from the junction box are transmitted to the acquisition system with cable connections. The signals from the accelerometers, displacement, and the pressure transducers are input to charge amplifiers, while the strain gages are connected to dynamic strain amplifiers to convert the voltage signal. These voltage signals are routed to the digital data acquisition system. The data acquisition system has a minimum of 16 bit resolution.

The signal level of each transducer is checked prior to the test to adjust the gains of the charge amplifiers for the accelerometers and pressure transducers. The dynamic strain amplifiers are balanced and appropriate sensitivities are selected. The spectrum of each signal is monitored during the test to verify the recording process and the adequacy of the level of data signals.

5.4.3 Process for Determining Frequency, Modal Content and the Maximum Values of Response

The initial reduction of the data is performed during the test to determine whether or not the responses are within the acceptable limits. Spectrum analysis is used to analyze the natural frequencies and the vibratory characteristics of each component to compare to the results from the pre-operational vibration assessment program (See Section 4.0). The maximum stress values are also calculated to confirm the structural integrity.

5.4.4 Bias Errors and Random Uncertainties

Bias error and uncertainties depend on the accuracy of both the acquisition system and the method used for the reduction of data. The accuracy of the data acquisition is primarily a function of instrument error and the accuracy of the data reduction is a function of the number of data samples, the bandwidth, etc. These bias errors and random uncertainties are defined by the specification for the data acquisition system and signal processing equipment. The total instrument errors are calculated using a root sum of the squares (RSS) method prior to hot functional testing. Sampling and averaging methods described in Section 5.4.1 combined with high quality sensors and modern digital recording minimize the random and bias errors.

5.5 Acceptance Criteria for the Tests

The RMS response of the RV internal component is determined by calculation from the captured time waveform or from the integration of the PSD for specific frequency bands for each of the transducers mounted on the RV internals. This vibration amplitude and stress response is compared to the pre-operational theoretical values and the acceptance criteria identified for each component in Section 4.0. The stresses must show sufficient safety margins based upon the design fatigue curves presented in Figure 4-21. Further, the theoretical and measured values for the natural frequencies of the RV internal components are compared to verify that the structural modeling has accurately accounted for the hydrodynamic mass and stiffness of the components.

The acceptance criteria will account for transducer location, operating conditions for each test, uncertainties and biases, and margins to be added for conservatisms to ensure that the allowable fatigue stress will not be exceeded. The best estimate stress values determined in Section 4.0 will be used as a basis for comparison with the measured values for evaluating the accuracy of the FIV predictive methods. The peak stresses as well as the distribution of stresses throughout the component are determined by the analytical solutions. Due to practical considerations, such as situations where peak stresses occur at welds or at threaded joints where strain gages cannot be positioned, difficulties in accessing a desired location of peak stress, or difficulties in routing of instrument cables, the instrumentation may have to be located in non-peak stress positions. In these cases, adjustments will be made to scale the measured strains and resulting stresses to the peak stresses for the component. These biases and uncertainties will be taken into consideration when establishing the acceptance criteria for the HFT instrumentation.

The impact of the uncertainties and bias associated with the instrumentation and other equipment that will be used to perform the HFT with the acceptance criteria defined above is not known at this time. When the instrumentation and data acquisition system have been designed, this bias and uncertainty will be incorporated in a manner that will not diminish the criteria established above.

The HFT is acceptable if there is no evidence of excitation to the RV internal components due to fluid-elastic instability, acoustic resonance, and vortex-shedding lock-in. Because of the characteristics of the RCS design, vibrations of the RV internals are expected to be created primarily from random turbulence and acoustic pressure fluctuations associated with the RCP vane passing frequencies and the low frequency loop acoustics. Accuracy within a factor of 2.0 is expected for the vibrations induced by turbulence. Because the magnitude of the acoustic pressure fluctuations are verified at the time of HFT, it is difficult to estimate the degree of accuracy expected for the vibration associated with this source of excitation.

5.6 Evaluation Plan for the Test Data

Tables of the maximum allowable test values will be generated for the sensors for use in the detailed test procedures. These maximum allowable test values will be developed based upon consideration of the bias and uncertainties of the instrumentation described in the acceptance criteria of Section 5.5. These maximum allowable test values will provide guidance for the test operators when they are conducting the HFT and allow the operators to determine the margins between the sensor values being measured and the allowable values as the tests are progressing.

If deviation between the theoretical prediction and the measured values is observed, then these differences will be evaluated for impact on the integrity of the RV internals. If necessary, appropriate changes will be made to the theoretical evaluation to obtain an agreement in the response of the RV internals that are deemed critical to the integrity of the RV internals. This could include revising the structural model to consider a different hydrodynamic mass and stiffness, damping ratios, or to correct for the magnitude and coherence of the forcing function through the current definitions of the PSDs, correlation length or convective velocities.

As described in Sections 4.2.7 and 4.2.8, the response of the lower internals is primarily dominated by the pendulum mode [ ], and this mode has the most dynamic influence on the excitation of the fuel bundle. The flow excitations of the CB shell modes do not create significant stress in the CB members or excitation of the fuel bundle. Greater attention is given to the FIV inputs that are most influential in obtaining agreement with the response of the pendulum mode of the lower internals. Similar reasoning is applied to the other RV internal components.

6.0 INSPECTION PROGRAM

6.1 Principles of the Inspection Program

The inspection program for the RV internals involves visual inspections before and after the pre-operational tests. The internals are removed from the RV and placed on a storage stand in the reactor cavity for inspection. The accessible areas of the RV internals that are visually examined are:

- The fastening devices.
- The bearings surfaces.
- The interfaces between the RV internal components that are most likely to reveal relative motions and wear.

The inside of the RV is also visually examined for abnormalities.

The RV internals is visually examined with 5 to 10X magnification. Non-destructive surface examinations are used to inspect the welds of the RV internals.

The integrity of the RV internals is considered adequate and passes the inspection program phase of the comprehensive vibration assessment program if no indication of abnormally large vibration amplitudes or excessive wear is detected.

6.2 Inspection Plan

Visual inspections of the U.S. EPR RPV and its internals adhere to the guidelines and requirements provided by the 2004 edition of the ASME Section III, Paragraph NG-5111 and the methods defined in the ASME Section V, Article 9. The visual inspections "VT-1" and "VT-3" required by ASME Section XI, Subsection IWB-2500, Table IWB-2500-1 for the examination categories of the reactor vessel and the core support structures are followed to fulfill the requirements of the inspection program of RG 1.20. The acceptance criteria for these nondestructive surface examinations are provided in Table 6-6 and are used to inspect the surfaces and welds of the components identified in Tables 6-1 through 6-5.

Considering that the RV lower and upper internals are stored on the same stand, the inspections are performed in the following five steps:

1. Upper internals on the storage stand.
   Inspection of the whole accessible areas of the upper internals. Table 6-1 details the necessary inspections.
2. Lower internals in the RV.
   Inspection of the inside of the lower internals. Table 6-2 details the necessary inspections.
3. Lower and upper internals on the storage stand.
   Inspection of the outside of the lower internals. Table 6-3 details the necessary inspections.

4. Lower and upper internals on the storage stand.
   Inspection of the RV inside. Table 6-4 details the required inspections.
5. RV head on its storage stand.
   Inspection of the RV head inside. Table 6-5 details the required inspections.

Table 6-1—Visual Inspection of the Upper Internals on their Stand

Component	Sub-component	Inspection
Top surfaces of the upper support assembly.	CRGA housing.	Presence and condition of the bolts and their locking cups
	LMP thimble upper housing	Presence and condition of the bolts and their locking cups
	Head and vessel alignment pins	Presence and condition of the bolts and their locking bars
	Flange	Aspect of the bearing area
Bottom surfaces of the upper support assembly	Normal columns, LMP columns and accessible CRGA columns	Presence and condition of the bolts and their locking cups
	Flange	Hold down spring contact area
CRGA columns	Accessible guide tubes for instrumentation lance finger	Bracket fastening. Presence and condition of the bolts and their spot welds
UCP top surface	CRGA columns	Aspect of the flange / CRGA pin interface
	UCP guide pin inserts	Presence and condition of the bolts and their locking cups Aspect of the stellited surfaces
UCP bottom surface	Normal columns and LMP columns	Presence and condition of the bolts and their locking bars
	CRGA pins	Presence and condition of the locking device
	Guide tubes for instrumentation lance finger	Bracket fastening inside the UCP. Presence and condition of the bolts and their spot welds
	Upper fuel pins	Presence and condition of the pins and their spot welds

Table 6-2—Visual Inspection of the Inside of Lower Internals (In RV)

Component	Sub-component	Inspection
Core barrel flange: top surface	Head and vessel alignment pins	Presence and condition of the bolts and their locking bars
	Hold down spring contact area	Surface aspect
Heavy reflector top	UCP guide pins	Presence and condition of the bolts and their locking cups Aspect of the stellited surfaces
	Tie rods	Presence and condition of the nuts and their locking devices
Lower support plate	Access plug fasteners	Presence and condition of the bolts and their locking bars
	Lower fuel pins	Presence and condition of the pins and their spot welds

Table 6-3—Visual Inspection of the Outside of Lower Internals (On Their Stand)

Component	Sub-component	Inspection
Irradiation baskets	Fasteners	Presence and condition of the bolts and their locking bars
Radial key inserts	Insert fasteners	Presence and condition of the bolts and their locking bars
	Stellited surfaces of the inserts	Surface aspect

Table 6-4—Visual Inspection of the RV Inside

Component	Sub-component	Inspection
RV flange	Contact surface with the lower internal flange	Surface aspect
Outlet nozzles	Potential contact surface with the lower internal nozzles	Surface aspect
Radial keys	Insert fasteners	Presence and condition of the bolts and their locking bars
	Stellited surfaces of the inserts	Surface aspect

Table 6-5—Visual Inspection of the RV Head

Component	Sub-component	Inspection
RV head flange	Contact surface with the upper internal flange	Surface aspect
Adaptors	Thermal sleeves	Amplitude of vertical displacement

Table 6-6—U.S. EPR RPV and Internals Visual Inspection Plan

Parts Examined	Examination Category	Examination Method	Acceptance Criteria	Extent
Interior of Reactor Vessel	Category B-N-1	Visual, VT-3	IWB-3520.2	Surface
Interior Attachments to Reactor Vessels	Category B-N-2	Visual, VT-1	IWB-3520.1	Welds
Welded Core Support Structures	Category B-N-2	Visual, VT-1	IWB-3520.1	Welds
Removable Core Support Structures	Category B-N-3	Visual, VT-3	IWB-3520.2	Surface

Note(s) for Table 6-6:

1. The ASME Code, Section XI, Table IWB-2500-1 prescribes a VT-3 examination method for the B-N-2 examination category of the welded core support structures. To provide a more rigorous examination method, beyond that required by the ASME code for these parts, the examination method VT-1 and the corresponding acceptance criteria (IWB-3520.1) will be followed for the pre-service inspection of the RPV internals following hot function testing.

7.0 CONCLUSION

A comprehensive vibration assessment program for the U.S. EPR RV internals is established in accordance with Reference 1 and is described in the body of this report. The vibration assessments of the RCS piping systems and the attached piping systems of the RSG, the RSG upper internals, and the RSG tube bundle are provided in Appendix A, Appendix B, and Appendix C respectively.

The design of the U.S. EPR RV internals is derived from French N4 and German Konvoï designs. However, the U.S. EPR RV internals include new features that could introduce some changes in the vibratory behavior compared to the reference units. AREVA NP has classified the RV internals as "prototype" consistent with Reference 1.

AREVA NP has implemented a comprehensive vibration assessment program to verify the integrity of the U.S. EPR reactor internals that follows the recommendations of the Reference 1 for "prototype" reactor internals. This vibration assessment program is divided into three stages consisting of three sub-programs:

- Theoretical analyses and model tests that constitute the vibration and stress analysis program.
- Pre-operational tests with dedicated temporary instrumentation that constitute the vibration and stress measurement program.
- Inspection of the RV internals after pre-operational tests that constitute the inspection program.

The vibration and stress analysis program is based on both experimental and theoretical approaches. The goal of the analysis program is to predict the vibratory behavior of the RV internal vibration and to evaluate other potential phenomena that could influence this behaviour. The predicted vibration amplitudes are acceptable and are not considered detrimental to the integrity of the U.S. EPR RV.

Permanent VMS instrumentation that allows follow-up measurements during full power operating conditions is complemented by a large array of temporary instrumentation during the pre-operational testing phase of the vibration and stress measurement program. These temporary and permanent instrumentation systems enable a more accurate assessment of the vibratory behavior of the RV internals by providing actual data that is used, if needed, to refine the computation models. The vibration and stress measurement program is followed by an extensive inspection program that consists of visual inspection of parts and surfaces that could reveal signs of unexpected vibrations.

If discrepancies are identified during the pre-operational testing between the vibration analyses and the measurement programs, a reconciliation of the analysis program will be made and the final comprehensive vibration assessment report for the U.S. EPR RV internals will demonstrate agreement between the analysis and the measurements. The validation of the vibration behavior of the U.S. EPR RV internals establishes the U.S. EPR reactor internals as a valid prototype.

8.0 REFERENCES

1. U.S. Nuclear Regulatory Guide 1.20 (Rev 03), "Comprehensive Vibration Assessment Program for Reactor Internals during Preoperational and Initial Startup Testing," March 2007.
2. Blevins, Robert D., Flow-Induced Vibrations, 2nd edition, 2001.
3. Vibrations des structures – Interactions avec les fluides – Sources d'excitations aléatoires - R.J. GIBERT – Eyrolles Editions, 1988.
4. M. K. Au-Yang, "Flow-Induced Vibration of Power and Process Plant Components." New York: ASME Press, 2001.
5. NRC Regulatory Guide 1.207, "Guidelines for Evaluating Fatigue Analyses Incorporating the Life Reduction of Metal Components Due to the Effects of the Light-Water Reactor Environment for New Reactors," March 2007.
6. NUREG/CR-6909 (ANL-06/08), "Effect of LWR Coolant Environments on the Fatigue Life of Reactor Materials," February 2007.
7. B. Brenneman, "Random Vibrations Due to Small-Scale Turbulence with the Coherence Integral Method," ASME Journal of Vibration, Acoustics, Stress, and Reliability in Design, Vol. 109, April 1987.
8. A. Powell, "On the Fatigue Failure of Structures Due to Vibrations Excited by Random Pressure Fields," Journal of Acoustical Society of America, Vol. 30, No. 12, 1958, pp. 1130-1135.
9. ASME Boiler and Pressure Vessel Code, 2004 Edition with no Addenda
   a. Section III, Appendix N-1300 (non-mandatory appendix)
   b. Section II, Part D, Design Stress Intensity Values, Allowable Stresses, Material Properties.
   c. Section III, Appendix I.
10. Regulatory Guide 1.68 Revision 3, "Initial Test Programs for Water-Cooled Nuclear Power Plants," March 2007.
11. Regulatory Guide 1.70 Revision 3 "Standard Format and Content of Safety Analysis Reports for Nuclear Power Plants," November 1978.
12. ASME OM-S/G 2007, "Operation and Maintenance of Nuclear Power Plants," Part 3
13. R.M. Baldwin and H.R. Simmons, "Flow-Induced Vibration in Safety Relief Valves," ASME Journal of Pressure Vessel Technology, Volume 108/267, August 1986.
14. "Impedance-Coupled Valve and Fluid System Instability," John Lynch, Advances in Mathematics, Computations and Reactor Physics, Volume 3, International Topical Meeting among American Nuclear Society, Atomic Energy Society of Japan, and European Nuclear Society, 1991.
15. NUREG-0800 U.S. Nuclear Regulatory Commission Standard Review Plan 3.9.2 Dynamic Testing and Analysis of Systems, Structures, and Components, March 2007.
16. MacLeod, Greg and David Weaver, "Entrance Port Rounding Effects on Acoustic Resonance in Safety Relief Valves," ASME PVP Volume 389, Flow-Induced Vibration – 1999.

17. S. Ziada, S. Shine, "Strouhal Numbers Of Flow-Excited Acoustic Resonance Of Closed Side Branches," Journal of Fluids and Structures, Volume 13, Issue 1, Pages 127-142, January 1999.

18. "Formulas For Stress and Strain," Fourth Edition, R. J., Roark.

19. "A Wave Decomposition Method for the Active Control of Sound Absorption: Theory and First Experimental Results," Marco Norambuena, Jakob, Andre, Moser,Michael, Institute fur Stromungsmechanik and Technische Akustik, Technische Universitat Berlin, Eisnsteinufer 25, D-10587.

20. "Error Analysis of Two-Microphones Measurements in Ducts with Flow," Abom, Mats and Boden, Hans, Department of Technical Acoustic, Royal Institute of Technology, S-10044 Stockholm, Sweden.

21. K.M. Bourcher, C.E Taylor, and M. Yetisire, "Vibration and Impact Forces Due to Two-Phase Cross-Flow in U-Bend Region of Heat Exchangers," *Proceedings of Sixth International Conference on Flow-Induced Vibration*, London, UK, pp. 404-411.

22. M. J. Pettigrew, and C.E. Taylor, "Two Phase Flow-Induced Vibration," *Technology for the 90s*, ASME Special Publication, Edited by M. K. AuYang, 1993.

23. K. Hirota et al, "Dynamics of In-Line Tube Array in HCFC-123 Two-Phase Flow," *Proceedings 4th International Symposium in Fluid-Structure Interaction*, Vol. II, ASME AD, Vol. 53-2, pp. 399-420, Edited by M.P. Paidoussis, 1997.

24. M. J. Pettigrew and D. J. Gorman, "Vibration of Heat Exchanger Bundles in Liquid and Two-Phase Cross-Flow," *Flow-Induced Vibration Guidelines*, ASME Special Publication PVP-52, edited by P. Y. Chen. 1981.

25. Chandler, C. Kaye, "Methods of Determining a Damping Ratio from a Simple Impact Test," Paper PVP2005-71041, Proceedings of ASME Pressure Vessels and Piping Division Conference, July 17-21, Denver, Colorado.

26. EPRI NP-4559, "Flow-Induced Vibration of Steam Generator Tubes," May 1986.

27. EPRI Steam Generator Reference Book, May 1985.